J Solid State Electrochem (1999) 3: 97–103

ORIGINAL PAPER

Stefan Machill · Takahisa Shodai · Yoji Sakurai
Jun-ichi Yamaki

Electrochemical and structural investigations of the reaction of lithium with tin-based composite oxide glasses

Received: 2 October 1997 / Accepted: 3 July 1998

Abstract Tin-based composite oxide materials have received considerable attention as potential anode materials for rechargeable lithium batteries. In this contribution we present the results of our investigations of the $SnO—B_2O_3—P_2O_5$ system. We have investigated its electrochemical properties and especially its cycling performance. A focus of our interest was to explain the structural changes which occur during lithium cycling and their strong dependence on the preparation method. A part of the Sn—O component was converted into a very stable metallic phase. In addition, a decrease was observed in capacity owing to the formation of isolated and inactive tin grains. We also report on structural changes in the $B_2O_3—P_2O_5$ matrix.

Key words Lithium battery · Anode · Amorphous tin composite oxides · X-ray diffraction · Infrared spectroscopy

Introduction

A large number of materials and electrode concepts have been extensively studied over a long period with a view to replacing metallic lithium as the negative electrode in rechargeable batteries [1]. A novel material must meet several requirements. For a practical battery, it must be low in cost, easily available and not harmful to human life. The specific capacity and the potential should be close to that of metallic lithium.

S. Machill · T. Shodai (✉) · Y. Sakurai · J. Yamaki[1]
NTT Integrated Information & Energy Systems Laboratories, Tokaimura, Naka-gun, Ibaraki-ken 319-11, Japan

Present address:
[1]Institute of Advanced Material Study, Department of Molecular Science and Technology, Kyushu University, 6-1 Kasuga-koen, Kasuga-shi, Fukuoka 816, Japan

Work in this field has mainly focused on carbon-based materials. Such materials offer good cycleability because they form a lithium-ion-conducting passivation layer. A disadvantage is that a part of the initial charge capacity is consumed to form this protective layer.

In terms of other negative electrode materials, studies have been undertaken on lithium transition metal nitrides [2] and transition metal oxides or dichalcogenides [1, 3]. TiS_2, $WO_2$and MoO_2 have been specially proposed as anodes. However, these materials represent no serious challenge to carbon. Some of these materials have a high potential in comparison to lithium (Fig. 1), although this is not necessarily a disadvantage. Since the development of 4-V cathode materials [4] a new trend can be observed. Some materials first used as cathodes versus lithium are now being investigated as anodes in combination with 4-V cathodes. The Li/TiO_2system is well known and has been extensively examined [5]. Exnar et al. have reported novel 2-V TiO_2(anatase)/$LiCoO_2$ and TiO_2(anatase)/$LiNi_{0.5}Co_{0.5}O_2$ rocking chair lithium batteries [6–8]. They suggest that a 2-V system is more practical for microelectronic applications, especially in combination with photovoltaic recharging. Two-volt coin-type lithium ion cells based on either Nb_2O_5 or $Li_{4/3}Ti_{5/3}O_4/V_2O_5$ chemistries are already commercially available for memory backup use.

In principle, the disadvantages of metallic lithium cycleability can be avoided by using these materials. Nevertheless, it should be mentioned that none of these anodes has yet shown the high energy density properties demonstrated by batteries based on lithium metal.

Since the announcement of Fujifilms' Stalion battery, there has been intense discussion on the use of amorphous tin composite oxides as the anode materials for rechargeable lithium ion batteries [9–13]. SnO and SnO_2 also belong to this group of materials, which were first examined as cathodes [5, 14–16]. However, these compounds attained no practical importance as cathodes because of their low cell voltage.

The new composite oxide materials offer a higher theoretical volumetric and gravimetric capacity

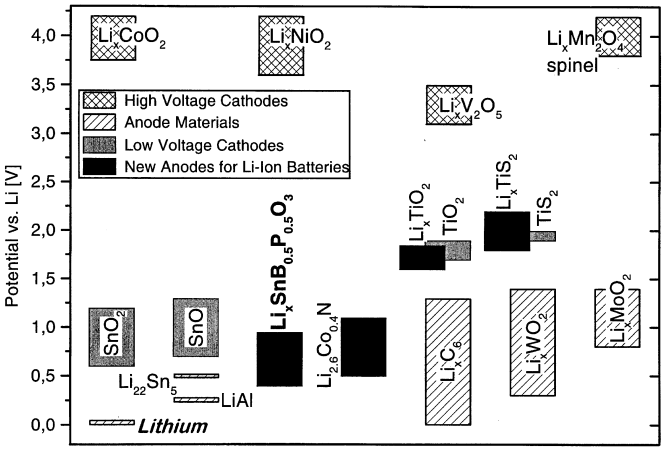

Fig. 1 Electrochemical potential of some electrode materials used in lithium batteries

(>600 mAh/g; 2200 mAh/cm^3 [9]) than carbon. However, the lithium storage mechanism is not yet completely understood. The observed storage of up to seven lithium atoms per atom of tin is not typical for intercalation systems. This is why some researchers suggest reduction to metallic tin followed by lithium alloying [10, 11, 17].

This study makes a contribution to clarify the lithium storage mechanism in $SnO—B_2O_3—P_2O_5$ composite oxide glasses by using Fourier transform infrared spectroscopy (FTIR) and X-ray diffraction (XRD) in combination with electrochemical measurements.

Experimental

Material preparation

We prepared several $SnB_xP_yO_z$ compositions (Table 1) by solid-state reactions at high temperatures. For synthesis, reagent grade SnO (Showa Chemicals), B_2O_3 with either P_2O_5 (both Kanto Chemical) or $Sn_2P_2O_7$ (Aldrich) were mixed in appropriate amounts and melted in a sintered alumina crucible under Ar. The oxygen-rich material $SnB_{0.5}P_{0.5}O_{3+x}$ was obtained by melting the starting materials in an Ar:O_2 (1:1) atmosphere. The furnace was heated at 200 °C/h to a final temperature of 1000 °C and held for 4 h. The cooling rate was about 200 °C/h. The product obtained was a compact glass that had a yellow colour which varied in intensity depending on the composition.

Table 1 Molar composition of the several investigated oxides

SnO	B_2O_3	P_2O_5	Composite oxide
1	0.25	0.25	$SnB_{0.5}P_{0.5}O_3$
1	0.3	0.2	$SnB_{0.6}P_{0.4}O_{2.9}$
1	0.2	0.3	$SnB_{0.4}P_{0.6}O_{3.1}$
2	0.25	0.25 $Sn_2P_2O_7$	$Sn_2B_{0.5}P_{0.5}O_4$
0.5	0.25	0.25	$SnB_{0.5}P_{0.5}O_3$

Part of the $SnB_{0.5}P_{0.5}O_3$ was treated by a single-roll quenching equipment (Nisshin-giken) The samples were melted at 1000 °C in Pt nozzle using radio-frequency heating, and then jetted by Ar gas pressure on a Cu roll (20 cm in diameter) at 2000–3000 rev/min. The atmosphere was Ar. Samples of the complete amorphous phase were obtained. The cooling rate was 10^4–10^5 °C/s.

Cell assembly

For electrochemical investigations the samples were ground and composite electrodes were formed by mixing the sample with 25 wt% acetylene black (Denki Kagaku) and 5 wt% polytetrafluoroethylene powder (Daikin) as binder, using an automatic agate mortar. The electrodes were rolled out between two cylinders and cut into pellets (15 mm in diameter, and about 0.3 mm thick).

The anode performance of the material was studied in coin-type cells (type R2320) using Li metal (Honjo Metal) as a counter electrode. A microporous polypropylene film (Celgard 3501, Hoechst Celanese) was used as a separator. The electrolyte we used was 1 M $LiClO_4$ in ethylene carbonate/1,2-diethoxyethane (Lipaste EDEE/1 Tomiyama Pure Chemicals).

The cell assembling was carried out in a dry air atmosphere (the dew point was less than −50 °C).

Measuring equipment

The charge/discharge behaviour of the cells was measured galvanostatically (current density = 0.5 mA/cm^2) in the 0.0–1.5 V range.

The structures were characterized by XRD (Rigaku RU-200) measurements using Cu $K\alpha$ radiation with a graphite monochromater. Step width was 0.02 ° and data acquisition time per step was 0.6 s. DS and SS were 1 ° and RS was 0.3 mm.

The FTIR spectra were measured in KBr pellets under a dry nitrogen atmosphere using a Perkin Elmer 1720X FTIR spectrometer.

For X-ray photoelectron spectroscopy measurements we utilized an ESCA-5400 system (Perkin Elmer) with a Mg $K\alpha$ X-ray source working at the exciting power of 400 W.

The samples containing lithium were prepared as follows. The coin-type cells were dismantled, the electrodes were washed with tetrahydrofuran, vacuum dried and then analysed. All these operations were carried out in a dry atmosphere.

Results and discussion

Structural characterization of materials

B_2O_3 and P_2O_5 are well known as glass network forming compounds. They form macromolecular chains which are strongly cross-linked by assembling tetrahedra (BO_4, PO_4) and triangles (BO_3) [18]. When SnO is added, its primary effect is as a network modifier. According to the Zachariasen theory, glass formation would be impossible with a SnO content of more than 50 mol% if the Sn cations act only as a network modifier. Investigations by Tick [19] and Xu and Day [20] have shown that some fraction of the Sn cations acts in a network forming role.

Figures 2 and 3 show the XRD patterns of the different oxide materials. The patterns in Fig. 2 are for various $SnO:B_2O_3:P_2O_5$ compositions. Figure 3 shows $SnB_{0.5}P_{0.5}O_3$ synthesized under different conditions.

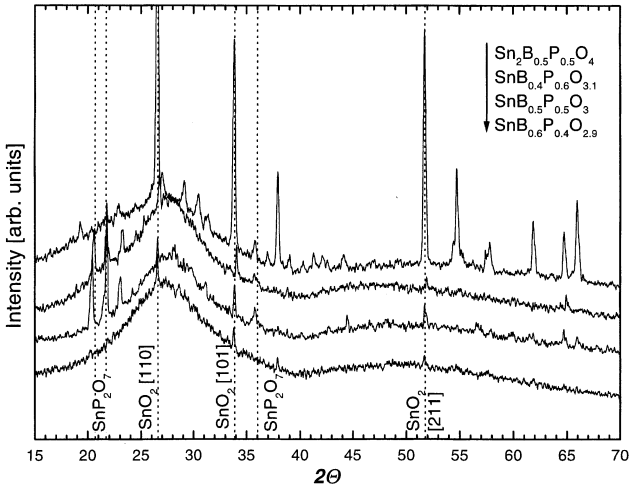

Fig. 2 X-ray diffraction (XRD) patterns of $SnO—B_2O_3—P_2O_5$ samples with various compositions

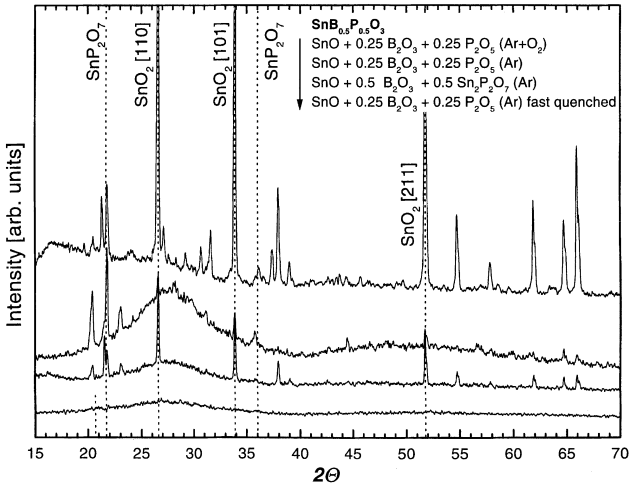

Fig. 3 XRD patterns of $SnB_{0.5}P_{0.5}O_3$ synthesized under various conditions

All the patterns show that the materials are in an almost amorphous state. Generally, we could observe a diffused broad halo around 27°. Beside it, the crystalline phase of the samples consists of phases of SnO_2 (cassiterite) and tin(IV) pyrophosphate (SnP_2O_7). The other phases could not be determined. In both cases the valency of tin is changed from Sn^{2+} in SnO to Sn^{4+} in SnO_2 or SnP_2O_7. In an inert gas atmosphere this oxidation is only possible if a corresponding reduction occurs. Investigations by X-ray photoelectron spectroscopy have shown that tin merely exists as Sn^{2+} or Sn^{4+}. Metallic tin could not be detected. By the analytical techniques used the inevitable reduction process occurring could not be determined.

The formation of SnP_2O_7 depends strongly on the amount of phosphorus. In the sample with the lowest proportion of P_2O_5 ($SnB_{0.6}P_{0.4}O_{2.9}$) the SnP_2O_7 phase could not be detected. The oxidation of SnO to SnO_2 seems to be independent of the composition. The SnP_2O_7 phase does not appear when there is a surplus of SnO ($Sn_2B_{0.5}P_{0.5}O_4$), but the intensity of the cassiterite lines is much greater.

The synthesis of $SnB_{0.5}P_{0.5}O_{3+x}$ in a mixed argon-oxygen atmosphere leads to a well-crystallized material. All the lines for cassiterite and tin(IV) pyrophosphate are confirmed in the XRD pattern of this material (Fig. 3).

The material synthesized by using $Sn_2P_2O_7$ as the phosphorus-supplying component shows a slightly higher intensity in the SnO_2 pattern. After the single-roll quenching treatment, the material was transferred in a completely amorphous state.

IR spectra of the various oxides are shown in Fig. 4. None of the samples shows any significant difference in the overall line shape of their spectra. Broad and continuous bands dominate the spectra. This indicates a glass-like system with a random structure.

The IR peak around 1360 cm^{-1} is attributed to B—O bond stretching in trigonal BO_3 units [21]. Furthermore, the band at 700 cm^{-1} is assigned to the bending of the B—O—B linkages in the borate network [22]. The band at 1250 cm^{-1} is related to the stretching vibration of P=O double bonds in polyphosphate anions. The absorption band near 1050 cm^{-1} has been assigned as the $P—O^-$ stretching vibration [23]. Xu and Day [20] associate this band with the P—O—Sn linkage in Sn—P—O—F glasses. The band at 550 cm^{-1} is attributed to the deformation of PO_4 tetrahedra [24]. The band expected for the Sn—O vibration in SnO_2 around 490 cm^{-1} can be observed but is weak.

There are only slight differences between the spectra for the various compositions. The band at 550 cm^{-1} changes in intensity depending on the amount of phosphorus. In addition, we can observe an increase in the intensity of the B—O stretching (1360 cm^{-1}) and the

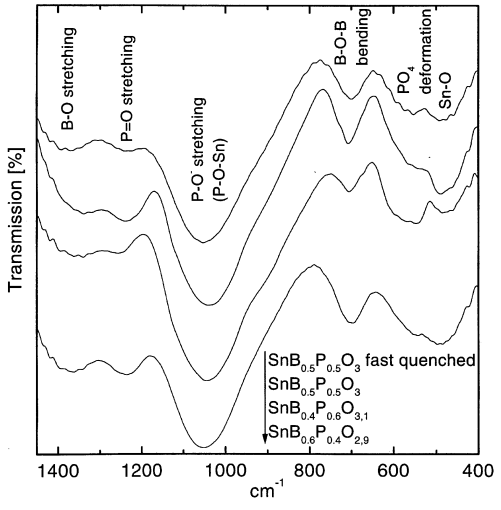

Fig. 4 Infrared (IR) spectra of $SnO—B_2O_3—P_2O_5$ samples with different compositions

B—O—B bending band (700 cm^{-1}) as the amount of boron increases.

Electrochemical characterization of materials

We examined the charge-discharge behaviour under constant current conditions between 1.5 and 0.0 V. Figure 5 shows the typical voltage-time behaviour of several materials during the first 1.5 cycles. The graphs are almost the same whatever the composition. In the first reduction step two clear voltage plateaus can be observed. The first plateau is in the 1–3 mol lithium region. A second appears around 5 mol of inserted lithium and is not seen so clearly. In all the subsequent charge-discharge steps only one plateau can be observed, as shown in the right part of Fig. 5.

The capacities of the first reduction step are not very different, around 7 Li/mol (1050 mAh/g). An exception is the graph for $SnB_{0.5}P_{0.5}O_{3+x}$. The large amount of 9 Li/mol (1150 mAh/g) can be inserted in this compound, which was melted in an Ar/O_2 mixture. This sample contains significant crystalline SnO_2, as shown in Fig. 3. It suggests that this material behaves in the same way as pure SnO_2 [11].

Around 3 mol lithium/mol oxide can be reversibly removed and cycled from the lithiated substrates. The rest of the initial capacity is irreversibly lost. The cycling performance of several $SnO—B_2O_3—P_2O_5$ compounds is depicted in Fig. 6. During the first 10 cycles, capacities fall to approximately 30–50% of their initial value. After that, over 40 cycles we can achieve relatively stable capacities between 50 and 170 mAh/g. This corresponds to less than 1 mol lithium/formula unit.

The inset in Fig. 6 shows the specific capacities related to the molar mass which seem to be independent of the composition, suggesting that the capacity is determined solely by the amount of tin in the matrix.

The cycling performance of the fast-quenched $SnB_{0.5}P_{0.5}O_3$ can be compared with that of the unquenched sample. The differences in structure give an improvement in the cycleability for the quenched sample from the 20th cycle.

Structural changes during lithium insertion

In order to explain the processes of lithium incorporation in tin-containing composite oxides we have investigated the changes in the structure of unquenched $SnB_{0.5}P_{0.5}O_3$ ($SnO—B_2O_3—P_2O_5$) during cycling, particularly during the first reduction step. The voltage-time characteristic for this material is given in Fig. 7. The corresponding X-ray patterns are shown in Fig. 8. The coin-type cells were disassembled after a 1 week rest time in order to guarantee homogeneous distribution of lithium in the matrix.

As shown in Figs. 5 and 7, most of the initial capacity is reduced irreversibly. The X-ray patterns in Fig. 8 show that at least some of the SnO_x component of the

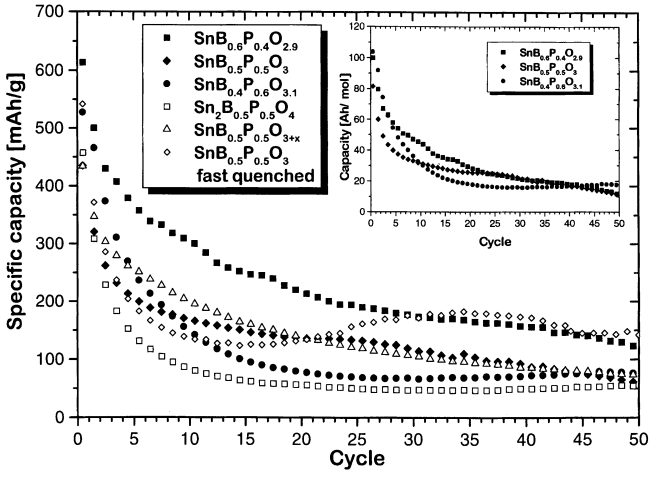

Fig. 6 Cycling performance of several $SnO—B_2O_3—P_2O_5$ composite oxides; $|i| = 0.5$ mA/cm^2; 0.0 V↔1.5 V

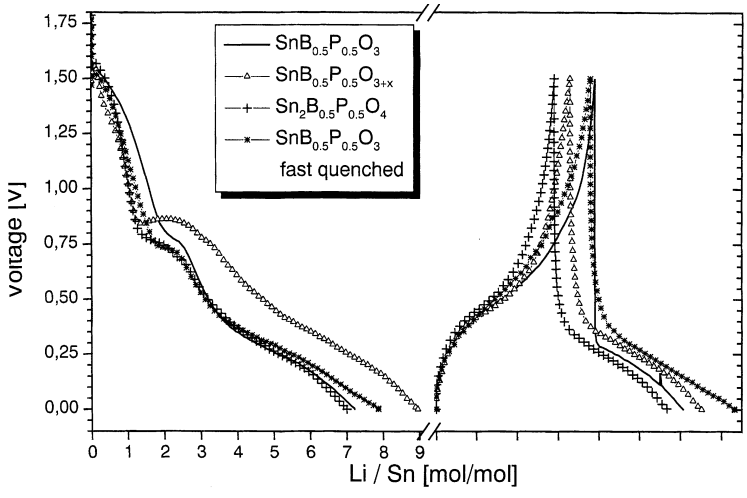

Fig. 5 Voltage-time behaviour of several $SnO—B_2O_3—P_2O_5$ composite oxides; $|i| = 0.5$ mA/cm^2

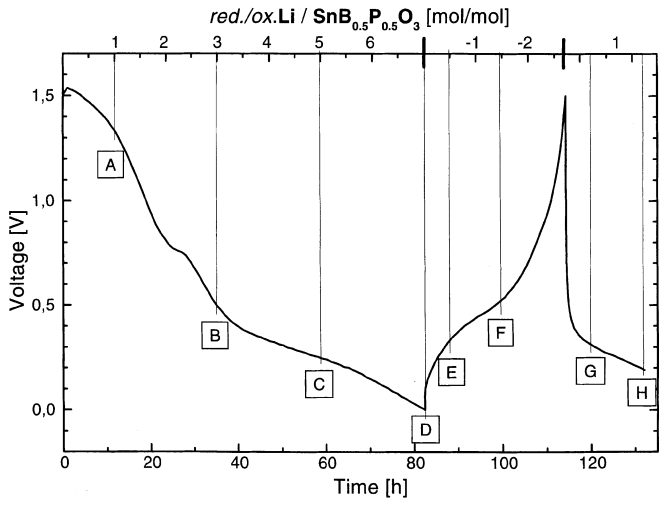

Fig. 7 Voltage-time behaviour of $SnB_{0.5}P_{0.5}O_3$ for the initial 1.5 cycles

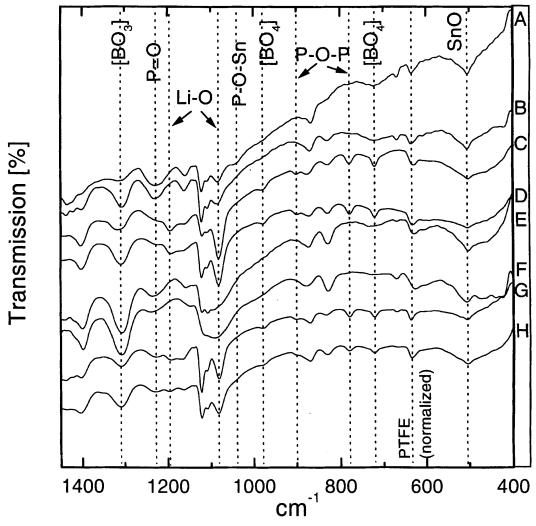

Fig. 9 IR spectra of $SnB_{0.5}P_{0.5}O_3$ for the initial 1.5 cycles (states A–H correspond to Fig. 7)

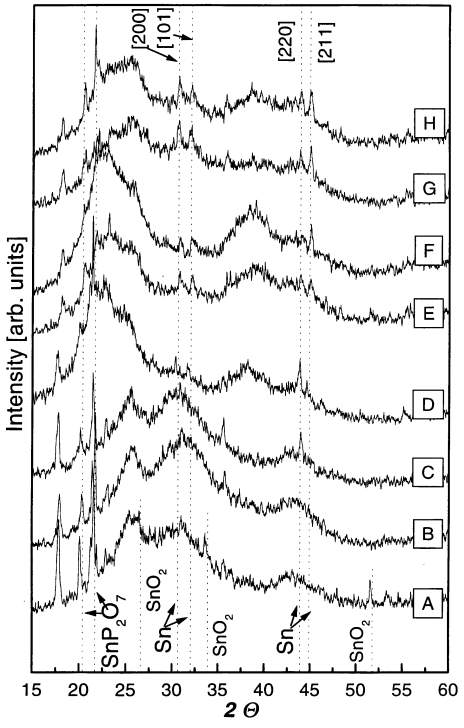

Fig. 8 XRD patterns of $SnB_{0.5}P_{0.5}O_3$ for the initial 1.5 cycles (states A–H correspond to Fig. 7)

composite oxide will be irreversibly reduced and metallic tin and amorphous Li_2O will be formed at the same time, also shown in Fig. 9. The formation of metallic tin can be observed during the initial reduction step, at least from state C.

Courtney and Dahn [10] describe the conversion of tin-containing composite oxides into binary Li—Sn alloy during cycling. They propose that the accumulation of the patterns of several Li_xSn_y alloys results in a broad halo around 22_∞ and 38_∞. We could only find these broad patterns in state D. By contrast, the X-ray patterns in states E–H indicate that the formed metallic tin is stable during lithium cycling. This means that a part of the formed metallic tin is isolated in the glass network and reduces the capacity. The SnP_2O_7 embedded in the network does not react with lithium.

Figure 9 shows IR spectra corresponding to the different lithium insertion states in the voltage-time behaviour (Fig. 7). The IR spectra have relatively weak absorption bands owing to the use of complete pellets, including acetylene black and polytetrafluoroethylene binder. Because of this, some additional bands can be observed in the spectra. All the spectra were normalized to the band at 630 cm^{-1} (PTFE). The changes in the spectra are discussed below.

The broad band at 500 cm^{-1} assigned to Sn—O decreases in intensity during the first reduction step. This confirms the result of the XRD investigations which revealed that the Sn—O bonds are broken during the simultaneous formation of the Li—O bonds. Guzman et al. [25] suggest that the bands at 1200 and 1080 cm^{-1} are Li—O stretching vibrations. They came to this conclusion as result of the lithium insertion in $MoO_3A0.5$-H_2O. These two bands disappear during the first oxidation state (E, F) and appear again in states G and H. This suggests that lithium can be stored in tin composite oxide anode materials by forming Li—O bonds. This means we can consider it to be an insertion material.

Several authors [26, 27] have reported on the changes in the IR spectra of B_2O_3 glasses when a modifier such as Li_2O is added. The absorption band at 1310 cm^{-1} characterizes the stretching of B—O bonds in BO_3 units. The main observation is the growth of two new bands at 730 and 980 cm^{-1}, attributed to the stretching of the

vibrations in BO_4 tetrahedral units. Balkanski et al. [21, 28, 29] describe the mechanism for the transformation of threefold coordinated boron centres into fourfold coordinated boron centres owing to the addition of Li_2O.

The change in the structure of the phosphorus network is mainly connected with the appearance of two new bands around 785 and 900 cm^{-1} which occur during the first reduction. These are attributed to the existence of P—O—P linkages in a glass network [20, 23]. By contrast, the P=O stretching vibration vanishes gradually during the initial reduction. The changes in the P—O bonds seem to be reversible and independent of the formation of metallic tin.

The band ascribed to $P—O^-$ stretching in P—O—Sn bonds disappears from states A to B. This can be explained in terms of the splitting of Sn^{2+} (Sn^{4+}) followed by a reduction to metallic tin. This process is not reversible and can be observed only in the initial step.

Any further indications with respect to the tin(IV) pyrophosphate are not provided by the IR spectra.

Conclusions

In our opinion, the following processes occur during the cycling of lithium on tin-containing composite oxides. The equations are schematic and do not represent reactions in a chemical sense. The stoichiometry and charge neutrality are not important in the equations.

Reductionprocess(lithiuminsertion)

$\Longleftrightarrow$

Oxidation process (lithium extraction)

$$\text{P—O—Sn—} \xrightarrow[\text{(irreversible)}]{} \text{P—O} \quad \text{Sn—} \tag{1}$$

$$\begin{matrix}\text{SnO}\\ \text{SnO}_2\end{matrix} \xrightarrow[\text{(irreversible)}]{} \text{Li}_2\text{O} + \text{Sn} \tag{2}$$

$$\text{Sn} \Longleftrightarrow \text{Li}_x\text{Sn}_y \tag{3}$$

$$\text{Sn—O} \underset{\text{(reversible)}}{\Longleftrightarrow} \text{Sn—O—Li} \tag{4}$$

$$[BO_3] \underset{\text{(reversible)}}{\Longleftrightarrow} [BO_4] \tag{5}$$

$$\text{P=O} \underset{\text{(reversible)}}{\Longleftrightarrow} \text{P—O—P} \tag{6}$$

$$\text{SnP}_2\text{O}_7 \quad \text{(inactive)} \tag{7}$$

In the first reduction step, the tin fragments which are incorporated in the glass network will be split off (Eq. 1). These fragments and the partially contained phase SnO_2 are reduced to metallic tin simultaneously with the formation of Li_2O (Eq. 2). The existence of metallic tin could be confirmed at every charge-discharge state. This means that part of the tin must be isolated because of its electrochemical inactivity. On the other hand, the storage of lithium in pure Li_xSn_y alloy phases could not be detected so clearly (Eq. 3). IR spectra show the reversible formation of Li—O bonds during every reduction period (Eq. 4), suggesting reversible lithium storage in the composite oxide matrix.

The effects of the incorporation of Li_2O in borate and phosphate glasses are well known and could be confirmed for our system. The change from threefold coordinated boron to fourfold coordinated boron as a result of the electrochemical lithium incorporation seems to be reversible (Eq. 5). In the phosphorus network a reversible change could be observed between P=O and P—O—P bonds (Eq. 6). Part of the tin is bound as SnP_2O_7. This material is inactive as regards the reversible storage of lithium (Eq. 7). Therefore the formation of this phase should be avoided.

The applicability of the tin-containing amorphous oxides as negative electrodes in rechargeable lithium batteries described above appears questionable. Compared with Fujifilms' materials the cycling performance of our materials is very poor. This is because of the difference in structure resulting from the different method of synthesis. The materials we investigated exhibited some structural characteristics which enabled us to examine structural changes during the initial reduction step. We hope this contributes to an understanding of the mechanism even if a number of points remain unclear.

Acknowledgements The authors would like to express their gratitude to Dr. I. Yamada for his continuous guidance and encouragement. They also wish to thank the members of their research group for helpful discussions.

References

1. Fauteux D, Koksbang R (1993) J Appl Electrochem 23: 1
2. Shodai T, Okada S, Tobishima S, Yamaki J (1996) Solid State Ionics 86–88: 785
3. Hossain S (1995) In: Linden D (ed) Handbook of batteries, chap 36. McGraw-Hill, New York, pp 36.1–36.77
4. Ohzuku T (1994) In: Pistoia G (ed) Lithium batteries. Elsevier, Amsterdam, pp 239–280
5. Ohzuku T, Takehara Z, Yoshizawa S (1979) Electrochim Acta 24: 219
6. Exnar I, Kavan L, Huang SY, Grätzel M (1997) J Power Sources 68: 720
7. Huang SY, Kavan L, Exnar I, Grätzel M (1995) J Electrochem Soc 142: L142
8. Kritl P, Kavan L, Fattakhova D (1997) J Solid State Electrochem 1: 83
9. Idota Y, Kubota T, Matsufuji A, Maekawa Y, Miyasaka T (1997) Science 276: 1395
10. Courtney IA, Dahn JR (1997) J Electrochem Soc 144: 2045
11. Courtney IA, Dahn JR (1997) Prog Batteries Battery Mater 16: 214
12. Brousse T, Retoux R, Herterich U, Schleich DM (1997) In: Holmes C F, Landgrebe A R (eds) Proceedings of the symposium on batteries for portable applications and electric vehicles, PV97–18. The Electrochemical Society, Pennington, pp 34–39
13. Courtney IA, Dahn JR (1997) J Electrochem Soc 144: 2943
14. Ilic DP, Schneider WE, Wiesener KH (1986) J Serb Chem Soc 51: 489

15. Ohzuku T, Takehara Z, Yoshizawa S (1978) Denki Kagaku 46: 407
16. Kahara T, Horiba T, Tamura K, Fujita M (1980) In: Owens BB, Margalit N (eds) Proceedings of the symposia on power sources for biomedical implantable applications and ambient temperature lithium batteries, PV80–4. The Electrochemical Society, Pennington, pp 300–308
17. Huggins RA (1997) In: Holmes C F, Landgrebe A R (eds) Proceedings of the symposium on batteries for portable applications and electric vehicles, PV97–18. The Electrochemical Society, Pennington, pp 1–18
18. Souquet JL, Kone A, Levy M (1990) In: Akridge JR, Balkanski M (eds) Theory and application of amorphous solids for electrochemical cells. Solid state microbatteries. Plenum, New York, pp 301–322
19. Tick PA (1984) Phys Chem Glasses 25: 149
20. Xu XJ, Day DE (1990) Phys Chem Glasses 31: 183
21. Deppe J, Balkanski M, Wallis RF, Massot M (1991) Mater Res Symp Proc 210: 125
22. Kamitsos EI, Karakassides MA, Chryssikos GD (1987) Phys Chem Glasses 28: 203
23. Hu L, Jiang Z (1994) Phys Chem Glasses 35: 38
24. Anma M, Yano T, Yasumori A, Kawazoe H, Yamane M (1991) J Non-Cryst Solids 135: 79
25. Guzman G, Yebka B, Livage J, Julien C (1996) Solid State Ionics 86–88: 407
26. Singh K (1997) Solid State Ionics 93: 147
27. Irion M, Couzi M, Levasseur A, Reau JM, Brethous JC (1980) J Solid State Chem 31: 285
28. Dzwonkowski P, Eddrief M, Julien C, Balkanski M (1991) Mater Res Symp Proc 210: 633
29. Massot M, Haro E, Oueslati M, Balkanski M (1989) Mater Res Symp Proc 135: 207